Waveguide efficient directional coupling and decoupling via an integrated plasmonic nanoantenna

Guillaume Blanquer, Vivien Loo, Nancy Rahbany, Christophe Couteau, Sylvain Blaize, Rafael Salas-Montiel, Yannick de Wilde, Valentina Krachmalnicoff

Waveguide efficient directional coupling and decoupling via an integrated plasmonic nanoantenna

GUILLAUME BLANQUER,[1] VIVIEN LOO,[1] NANCY RAHBANY,[1] CHRISTOPHE COUTEAU,[2] SYLVAIN BLAIZE,[2] RAFAEL SALAS-MONTIEL,[2] YANNICK DE WILDE,[1] AND VALENTINA KRACHMALNICOFF[1,*]

[1]*Institut Langevin, ESPCI Paris, Université PSL, CNRS, 75005 Paris, France*
[2]*Laboratory Light, nanomaterials & nanotechnologies – L2n*
University of Technology of Troyes (UTT) & CNRS ERL 7004
12 rue Marie Curie, Troyes, France
**valentina.krachmalnicoff@espci.fr*

Abstract: The development of integrated photonic devices has led to important advancements in the field of light-matter interaction at the nanoscale. One of the main focal points is the coupling between single photon emitters and optical waveguides aiming to achieve efficient optical confinement and propagation. In this work, we focus on the characterization of a hybrid dielectric/plasmonic waveguide consisting of a gold triangular nanoantenna placed on top of a TiO_2 waveguide. The strong directionality of the device is experimentally demonstrated by comparing the intensity scattered by the nanotriangle to the one scattered by a SNOM tip for different illumination geometries. The ability of the plasmonic antenna to generate powerful coupling between a single emitter and the waveguide will also be highlighted through numerical simulations.

1. Introduction

The development of integrated optical devices has promoted significant advancement in controlling light-matter interaction at the nanoscale. Such opto-electronic devices aim to perform and implement logical operations using optical components [1], which has led to a decrease in their size reaching a limit that conventional electronic circuits cannot endure. This is particularly promising, as technological and physical limits hamper the improvement of the computing capacities of conventional electronic processors, a problem that is overcome by integrated photonic devices [2]. Another advantage is their low energy consumption and low cross-talk compared to microelectronic devices [3]. In addition, integrated photonic circuits have important applications in the field of quantum optics and quantum information processing [4–8]. The main building blocks of quantum photonic circuits are single photon sources [9,10]. The development of such new technologies lies in the effective coupling of the light emitted by single emitters into optical waveguides, as well as the efficient communication between them [11,12]. An enhanced coupling of a single emitter to its environment can be achieved thanks to the use of plasmonic structures. The latter offer the advantage of strong field confinement and support surface plasmon polaritons (SPPs) with propagation lengths of several micrometers in the visible range. SPP-assisted energy transfer between emitters located up to 10 µm apart has been demonstrated on fully metallic SPP waveguides [13,14]. Such devices produce a strong attenuation of SPPs due to ohmic losses in the metal, which limits the communication distance between emitter and receiver and its efficiency. It was shown that hybrid structures comprising optical waveguides and embedded nanoantennas could be useful in overcoming this problem. Integrating a triangular nanoantenna on an optical waveguide demonstrated strong electromagnetic confinement at the apex of the triangle [15–17], and enhanced

photoluminescence of emitters [18]. V-shaped nanoantennas placed on dielectric waveguides showed strong directivity [19–21], and significant influence on the far-field emission diagram of fluorescent emitters [22], and both an efficient coupling and a strong directionality was achieved with Yagi-Uda nanoantennas made of gold nanorods integrated on dielectric waveguides [23]. Regarding the possibility to position precisely fluorescent dipole emitters at specific locations on a photonic integrated circuit, besides the manipulation of active fluorescent probes with a scanning probe microscope [24,25], it has been recently shown that direct laser writing based on two-photon polymerization is an attractive novel method to integrate nanoemitters in a controlled manner on optical glass waveguides [26], and that it can benefit from the hot spots formed around plasmonic nanostructures [27].

In this work, we develop a device made up of a hybrid nanoantenna/dielectric waveguide (DWG) aiming to couple the light emitted by a single photon source and potentially achieve efficient communication with a distant receiver. We choose a system consisting of a triangular gold nanoantenna deposited on a titanium dioxide (TiO_2) DWG. The advantage of the dielectric nature of the waveguide is that it allows light propagation to distances much greater than those provided by SPPs. In addition, the aim of the plasmonic nanoantenna, triangular shaped, is to improve the coupling between the emitter and the DWG, and to provide strong directionality of the coupled light with an easy to fabricate device with respect to more complex geometries.

Directionality is due indeed to mode matching at the base of the nanotriangle [17]. The mode propagating in the DWG excites hybrid plasmonic−photonic modes at the base of the nanotriangle. The electromagnetic energy is exchanged between the plasmonic mode in the nanotriangle and the photonic modes propagating in the DWG. The resulting mode becomes a predominantly-plasmonic mode. Due to the narrowing of the gold layer from the base to the apex of the triangle, this mode is concentrated at the nanotriangle's apex giving rise to a directional phenomenon. Changing the dimensions of the triangle will modify the coupling from and to the DWG.

Furthermore, placing two distant similar nanotriangles base-to-base on the DWG will allow to inject and decouple the confined light, achieving energy transfer from the emitter to the receiver via the DWG.

2. Experimental results

Our hybrid structure was fabricated by a two-step electron beam lithography (EBL) technique. We first start by fabricating the DWGs made of TiO_2 (length = 30 μm, width = 1 μm) on a glass substrate (e-beam dose = 140 pC cm^{-2}). After the EBL process, a 150 nm layer of TiO_2 is evaporated. The DWGs are slanted at their ends to avoid any Fabry-Pérot effect. The second more critical step involves the exact positioning of the triangular gold nanoantennas at the center of the DWGs. After ensuring perfect alignment of the DWGs, triangular regions of 500 nm base and 500 nm height are insulated in the EBL polymer (e-beam dose = 300 pC cm^{-2}). Then, a 30 nm layer of SiO_2 is evaporated, followed by a 50 nm layer of gold. The SiO_2 spacer is added to provide better index matching between the triangles and the DWGs and ensure better coupling [15,16]. In Fig.1, we show an optical image of the fabricated hybrid nanoantenna/DWG structures (a), as well as scanning electron microscope (SEM) images of double nanotriangles placed base-to-base on the DWG (b), and a single nanotriangle placed in the center of the DWG (c).

The strong directivity of the hybrid structure, comprising a single triangular nanoantenna, is demonstrated experimentally by measuring the decoupling efficiency as a function of the direction of light propagation in the DWG. Due to the asymmetric shape of the plasmonic triangular nanoantenna, we expect two different values of the decoupling efficiency. In order to characterize the directionality of the nanoantenna, we perform two measurements of the scattered intensity (using an EMCCD), corresponding to light propagating in the DWG from

the base side to the apex side of the triangle and vice-versa. As shown in Fig. 1 (d), we illuminate the DWG extremity by a focused laser beam beneath the sample. A portion of the incident light couples into the DWG and propagates towards the triangular nanoantenna where it decouples and scatters into the far-field. The comparison between the intensity scattered by the antenna in the two propagation directions is crucially related to the repeatability of the

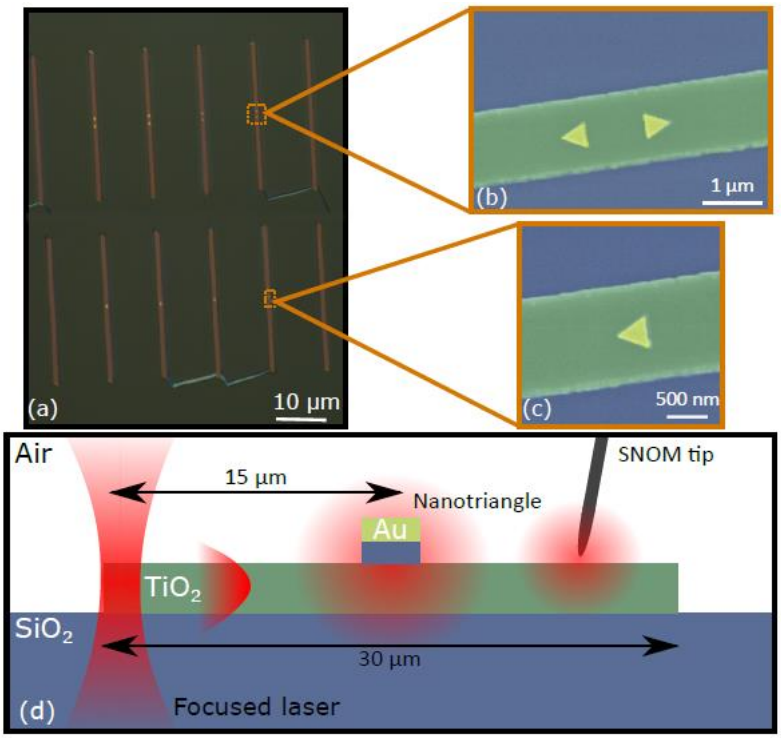

Fig. 1. (a) Optical image of the hybrid nanoantenna/DWG structures. Scanning Electron Microscope (SEM) images of (b) two nanotriangles placed base-to-base on the DWG, and (c) a single nanotriangle placed in the center of the DWG (false colors). (d) Sketch of the sample, the illumination geometry, and the SNOM tip. The light scattered by the nanotriangle and the SNOM tip is imaged on an EM-CCD camera.

experiment. The two cases are studied independently and therefore we cannot guarantee the exact same coupling of the laser in the DWG from both sides. Indeed, such coupling is affected by several hard to control parameters such as the position of the laser spot on the extremity of the DWG, the position of the focal plane with respect to the DWG and the roughness of its slanted ends. In addition, we are forced to move the sample and realign it whenever we want to change the illumination side of the DWG in the experiments.

In order to circumvent this problem, we compare the intensity of guided light scattered by the nanoantenna to the intensity scattered by a chemically-etched tungsten SNOM tip placed on the DWG. This results in four independent cases illustrated in Fig. 2 (a)-(d). For light propagating from the extremity of the DWG towards the base of the nanotriangle, the SNOM tip is placed either on the base-side (Fig. 2 (a)) or the apex-side of the triangle (Fig. 2 (b)). Similarly, for light propagating from the extremity of the DWG towards the apex of the nanotriangle, the SNOM tip is placed either on the apex-side (Fig. 2 (c)) or the base-side of the triangle (Fig. 2 (d)). We then extract the scattered intensity for both the nanoantenna and the SNOM tip which we utilize here as a reference.

To detail more, a laser of wavelength 600 nm is focused on the extremity of the DWG so that a fraction of the incident light is coupled to the DWG and propagates towards the nanotriangle as shown in Fig. 1d. We use an EMCCD Peltier cooled highly sensitive camera to image the sample through a microscope oil objective (100x, NA = 1.43), to finely adjust the position of the SNOM tip at the top of the DWG and to perform high sensitivity measurements of the intensity of the light scattered by the SNOM tip and the nanotriangles. For each configuration sketched in Fig. 2 (a)-(d), the SNO M tip is placed at the center of the DWG and scans a region of 600 x 600 nm^2 by steps of 75 nm, where each scanning line perpendicular to

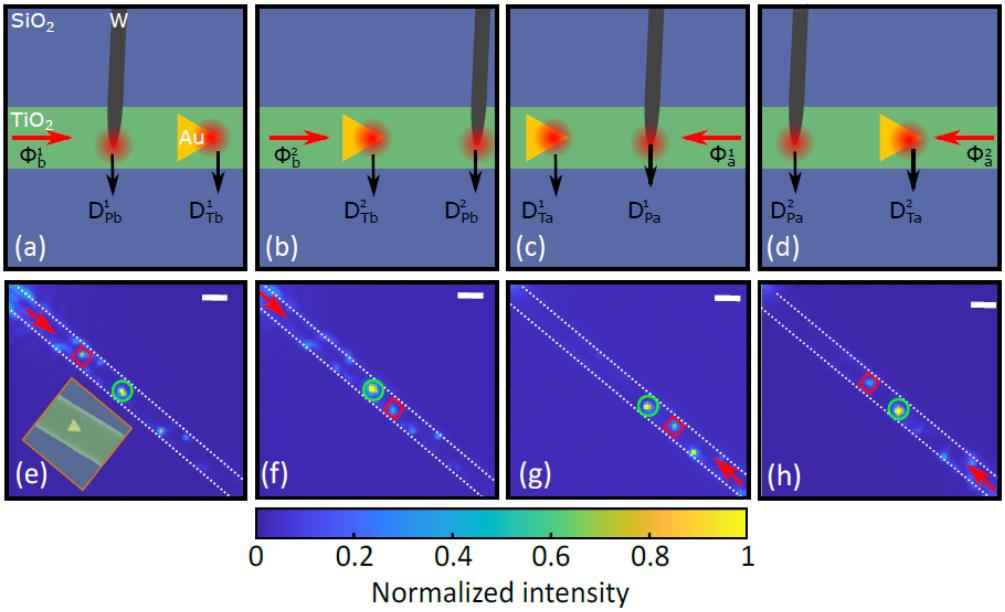

Fig. 2. (a) – (d) Sketches of the four different cases studied for characterizing the hybrid DWG. The direction of light propagation is indicated by the red arrow. For light propagating from the extremity of the DWG towards the base of the nanotriangle, the SNOM tip is placed on the DWG either (a) on the base-side, or (b) on the apex-side of the triangle. For light propagating from the extremity of the DWG towards the apex of the nanotriangle, the SNOM tip is placed on the DWG either (c) on the apex-side, or (d) on the base-side of the triangle. (e) – (f) Intensity maps corresponding to the four cases (a) – (d). Red squares represent the zones where the SNOM tip was displaced. Green circles represent the position of the nanoantenna on the DWG. White scale bars correspond to 1 µm.

the waveguide axis is scanned twice (back and forth). For each measurement point, an image is recorded via the EMCCD with an integration time of 10 s. This results in 128 images being recorded in every configuration. One of the 128 images is shown for each configuration in Fig. 2 (e) – (h). The zones where the SNOM tip was displaced are delimited by the red squares and the position of the nanoantenna on the DWG by green circles. Intensity hot spots on the edge of the waveguide are also visible. These hot spots are induced by defects that occurred during the manufacture of the sample.

3. Decoupling efficiency model

To calculate the decoupling efficiency values from the nanoantenna and the SNOM tip as a function of the light propagation direction, we use the fact that the scattering efficiency of the SNOM tip is constant at any position along the DWG. As shown in Fig. 2 (e)-(h), losses in the portion of the DWG between the tip and the nanotriangle are negligible with respect to the light scattered by the antenna and the tip. We also assume that the tip and the nanotriangle scatter the same modes of the propagating light in the DWG as verified by numerical simulations.

Based on these facts, we can now build a simple model to determine the decoupling efficiency values based on the scattered intensity measurements of both scatterers.

3.1 Light propagating towards the base of the nanotriangle

Let us consider first the case in which the light propagates from one extremity of the DWG towards the base of the nanotriangle. When the SNOM tip is placed on the base-side (Fig. 2 (a)), the intensity scattered by the SNOM tip is defined as:

$$D_{Pb} = \gamma_{Pb}\phi_b, \tag{1}$$

where ϕ_b is the intensity of the light propagating in the DWG and γ_{Pb} is the decoupling coefficient of the SNOM tip.

The intensity scattered by the nanotriangle is:

$$D_{Tb} = (1-\gamma_{Pb})\gamma_b\phi_b \tag{2}$$

where γ_b is the decoupling coefficient of the nanotriangle.

Similarly, when the SNOM tip is placed on the nanotriangle's apex-side (Fig. 2 (b)), the intensity scattered by the nanotriangle is:

$$\widetilde{D}_{Tb} = \gamma_b\tilde{\phi}_b \tag{3}$$

and the intensity scattered by the SNOM tip is:

$$\widetilde{D}_{Pb} = (1-\gamma_b)\gamma_{Pb}\tilde{\phi}_b \tag{4}$$

where $\tilde{\phi}_b$ is the intensity of the light propagating in the DWG.

Therefore, the decoupling coefficients of the SNOM tip and the nanotriangle can be expressed as:

$$\gamma_{Pb} = \frac{\chi_b - 1}{\chi_b + \frac{\widetilde{D}_{Tb}}{\widetilde{D}_{Pb}}} \quad \text{and} \quad \gamma_b = \frac{\chi_b - 1}{\chi_b + \frac{D_{Pb}}{D_{Tb}}} \tag{5}$$

where $\chi_b = \frac{D_{Pb}\widetilde{D}_{Tb}}{D_{Tb}\widetilde{D}_{Tb}}$.

3.2 Light propagating towards the apex of the nanotriangle

We can write analogue equations to describe the case in which light propagates from the extremity of the DWG towards the apex of the nanotriangle. One ends up with the following expressions for the decoupling coefficient of the SNOM tip γ_{Pa} and the decoupling coefficient of the nanotriangle γ_a:

$$\gamma_{Pa} = \frac{\chi_a - 1}{\chi_a + \frac{\widetilde{D}_{Ta}}{\widetilde{D}_{Pa}}} \quad \text{and} \quad \gamma_a = \frac{\chi_a - 1}{\chi_a + \frac{D_{Pa}}{D_{Ta}}} \tag{6}$$

where $\chi_a = \frac{D_{Pa}\widetilde{D}_{Ta}}{D_{Ta}\widetilde{D}_{Pa}}$. For the case in which the SNOM tip is placed on the side of the apex (Fig. 2 (c)), $D_{Pa} = \gamma_{Pa}\phi_a$ is the intensity scattered by the tip and $D_{Ta} = (1-\gamma_{Pa})\gamma_a\phi_a$ is the intensity scattered by the nanotriangle, with ϕ_a being the intensity of the light propagating in the DWG. Similarly, when the SNOM tip is placed on the side of the base of the nanotriangle (Fig. 2 (d)), $\widetilde{D}_{Pa} = (1-\gamma_a)\gamma_{Pa}\tilde{\phi}_a$ is the intensity scattered by the tip and $\widetilde{D}_{Ta} = \gamma_a\tilde{\phi}_b$ is the intensity scattered by the nanotriangle.

3.3 Decoupling efficiency measurements

The decoupling coefficients can now be calculated from Eqs. (5) and (6) using the experimentally measured scattered intensities from both the SNOM tip and the nanoantenna in

the different configurations discussed above. To do that, we first perform a Gaussian fit in the images recorded with the EMCCD camera on each scattered spot produced by the tip and the antenna to extract the corresponding values of the scattered intensity. These values are then averaged over each scan line, resulting in 8 measurement points per scanning area. Fig. 3 summarizes the obtained results. The dotted plots correspond to the decoupling coefficients of

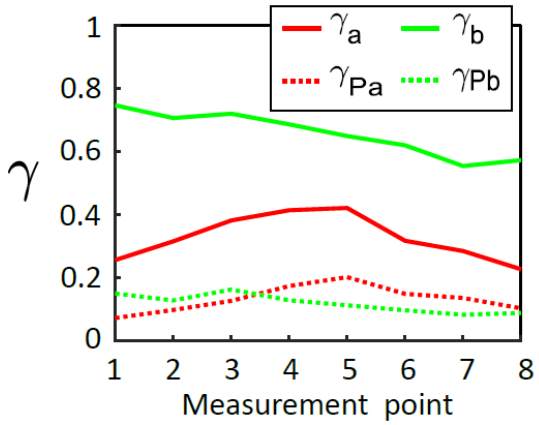

Fig. 3. Experimental values of the decoupling coefficients of the nanotriangle (solid plots) and the SNOM tip (dotted plots) calculated from the intensity maps. Green and red lines correspond to configurations where light is propagating towards the base and the apex of the nanotriangle respectively.

the SNOM tip for light propagating towards the base (green lines) and the apex of the nanotriangle (red lines). The average values are found to be $\gamma_{Pb} = 0.13 \pm 0.04$ and $\gamma_{Pa} = 0.12 \pm 0.03$. These similar values allow us to validate our hypothesis that the SNOM tip scatters the same fraction of light at any position on the DWG, which is independent of the light propagation direction. However, the solid curves, corresponding to the decoupling coefficients of the nanotriangle in both configurations, lead to the average values $\gamma_b = 0.66 \pm 0.07$ and $\gamma_a = 0.33 \pm 0.07$. As expected, the decoupling coefficients are strongly dependent on the light propagation direction through the DWG. The decoupling efficiency is thus much stronger for light propagating towards the base of the nanoantenna than in the opposite direction, proving the high directionality of our hybrid structure. This observation is confirmed by numerical simulations, performed in a broad spectral range and reported in Supplement 1, Fig. S1, that predict a decoupling ratio ≈ 2.2 at $\lambda = 600$ nm.

4. Numerical simulations: towards single-emitter coupling

Hybrid plasmonic/dielectric waveguides are particularly interesting when the question of coupling to the waveguide the light emitted by a fluorescent emitter is raised. As we will show with numerical simulations, the experimentally proven strong directionality of the light decoupled by our hybrid structure, is confirmed when a single emitter interacts with the hybrid DWG. We perform Finite-Difference-Time-Domain (FDTD) simulations to investigate the coupling into the DWG of the radiation emitted by a dipole emitter interacting with the nanotriangle. We expect to observe a similar directionality of the light from the dipole coupled by the nanoantenna into the DWG as the decoupled light observed experimentally. Figures 4 (a) and (b) present a schematic of our simulated structure, where a gold nanotriangle (base = height = 500 nm, thickness = 50 nm) is placed on a TiO_2 waveguide (width = 1 μm, thickness = 150 nm), with a 30 nm layer of SiO_2 in between (index of refraction $n = 1.46$). The waveguide is placed on a SiO_2 substrate. The index of refraction of the gold nanotriangle is taken from Yakubovsky et al. [28], and that of TiO_2 is taken from Sarkar et al. [29] A dipole emitter, oriented along the X-axis, is placed 10 nm away from the apex along the X direction

at a height of 55 nm on the top of the DWG. As demonstrated in previous studies [17,30,31] and tested by our simulations, this configuration has shown to lead to efficient coupling into the DWG. Perfectly Matched Layer (PML) boundaries are used to absorb incident electromagnetic waves and avoid reflections. Two 'frequency-domain field and power' flat monitors (schematized by the red lines M_1 and M_2 on Fig. 4 a,b) are placed along the X axis and perpendicular to the DWG, 10 µm away from the nanotriangle to avoid simulation artifacts (see Supplement 1, section 2 for a detailed explanation). These monitors are used to record the optical power (P_i) and allow us to extract the fraction of light injected in the DWG on both sides. A third monitor (a cube of 10 nm side) is placed around the dipole to detect the emitted power in its specific environment (P_E). This serves as a reference to which the light coupled into the waveguide on each side of the triangle is compared. The corresponding fraction of coupled light is thus calculated as $T_i = P_i/P_E$. The results are shown in Fig. 4c. The green plot represents the fraction of coupled light measured by the monitor M_1 located at the side of the base of the nanotriangle (T_1). We can clearly observe that up to 30% of the power radiated by the dipole is coupled to the DWG at the base of the nanotriangle, and that this efficient coupling is achieved over a large wavelength range (600 nm – 800 nm). This is made possible by the plasmonic nature and the shape of the nanoantenna, which increases the coupling efficiency into the DWG, and by the dielectric nature of the DWG which allows the propagation of guided light over long distances with minimum losses [32]. This agrees with the fact that, when a nanotriangle is illuminated through the DWG from the base-side, a hotspot characterized by high field concentration is produced at the apex, a phenomenon which does not occur in the reverse situation [16, 17]. Therefore a dipole placed close to the apex of the nanotriangle will couple to the DWG via the nanotriangle more efficiently than a dipole placed at the base. This is shown through a numerical comparative study of the two scenarios reported in Supplement 1, Fig. S3. We also note that the maximum coupling of 30% in the DWG is a significant enhancement in comparison with the situation in which the dipole radiates in the absence of the nanotriangle where a coupling of about 4 % is only achieved.

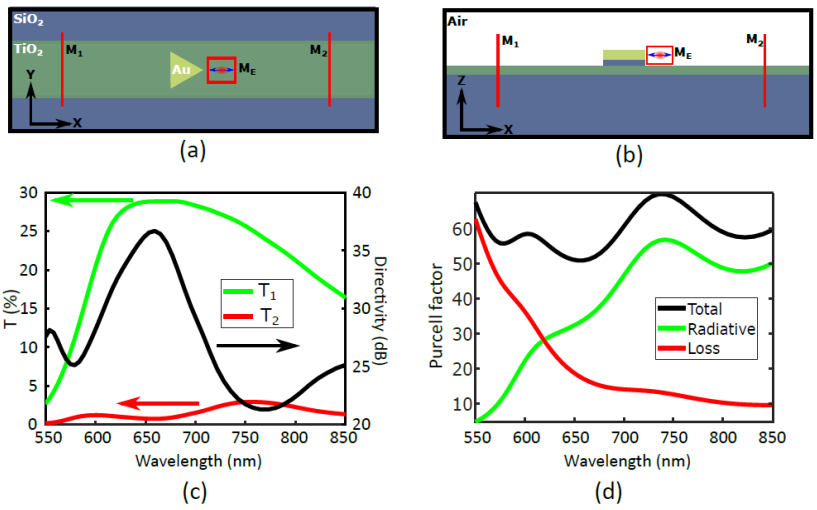

Fig. 4. (a) Simulation sketch top view ((b) cross view) of a dipole emitter placed at the apex of the nanotriangle and oriented along the X-axis. Red lines and square model the monitors $M_{1,2}$ used for the simulation. The SiO_2 layer (thickness 30 nm) and the coverslip are schematized in blue, the TiO_2 DWG (width = 1 µm, thickness = 150 nm) in green and the gold nanoantenna (base = height= 500 nm) in yellow. (c) Simulation results corresponding to the configuration described in a) for $M_{1,2}$ placed 10 μm away from the nanotriangle along the X-axis. Green and red plots correspond to the fraction of light coupled in the DWG when the light propagates towards the base and the apex of the nanotriangle respectively. Black plot: directivity D of the injection in the DWG. (d) Purcell factor (black curve), radiative (green curve) and non-radiative (red curve) components computed for the configuration described in (a).

On the other hand, we notice that only a tiny percentage of the power radiated by the dipole is coupled in the DWG on the opposite direction (T_2). Numerical values of the directivity $D = 10 \cdot \log(T_1/T_2)$ are shown by the black line in Fig. 4 c. It can be clearly observed that the directivity has a maximum at 660 nm, which corresponds to the optimization wavelength.

In order to account for the efficiency of the device, we computed the Purcell factor which characterized the enhancement of the Local Density of States (LDOS) at the position of the dipole. The results of the computation for the total Purcell factor and its radiative and non-radiative contributions is shown in Fig. 4 d. At λ = 600 nm the Purcell factor is around 55 with a balanced contribution of the radiative and non-radiative components.

5. Conclusion

In this work, we developed a hybrid optical system consisting of a gold nanotriangle deposited on a TiO_2 dielectric waveguide. The importance of this hybrid structure is that it makes use of both the plasmonic nature of the nanoantenna and the dielectric nature of the waveguide to attain high coupling efficiency and directivity, achieving strong confinement of the incident light and propagation to large distances with small losses. The structure was first characterized experimentally by comparing the intensity scattered by the nanoantenna and a SNOM tip, as a function of the direction of the injection of light in the DWG. This allowed us to extract the decoupling efficiency of the nanotriangle and demonstrate its directionality. FDTD simulations were carried out to characterize the coupling with a single dipole emitter. It was shown that the nanotriangle couples light more efficiently towards its base, demonstrating directivity of almost 40%. The strong dependence of the resonance wavelength and the directivity on the dimensions of the nanoantenna suggest that different types of hybrid structures with different sizes, shapes and materials can be studied aiming to reach higher coupling efficiencies. Moreover, our experimental and modeling work highlights the ability of this hybrid photonic device to perform energy transfer, over large distances, between two quantum emitters. To this aim, two nanoantennas could be fabricated on the same DWG (see Fig. 1b), one to optimize the coupling of an emitter to the DWG and the other to couple the light in the DWG to a receiver. A future development will be to place single dipole emitters precisely at the electromagnetic hot spots of the antennas which should be feasible by means of photopolymerization methods [26,27,31, 33,34]. In this way one should be able to experimentally demonstrate the coupling between two quantum emitters located far apart on a DWG. This work paves the way to achieve efficient energy transfer over considerably large distances on an integrated optical device, which can lead to promising improvement in the field of quantum information processing.

Acknowledgments. This research was supported by Emergences de la Ville de Paris 2015 and the LABEX WIFI (Laboratory of Excellence within the French Program Investments for the Future) under references ANR- 10-LABX-24 and ANR-10-IDEX-0001-02 PSL*. Samples were fabricated using the Nanomat' platform partly funded by the Grand Est region and the FEDER funds.

Disclosures. The authors declare no conflicts of interest.

Data availability. Data underlying the results presented in this paper are not publicly available at this time but may be obtained from the authors upon reasonable request.

Supplemental document. See Supplement 1 for supporting content.

References

1. C. Sun, M. T. Wade, Y. Lee, J. S. Orcutt, L. Alloatti, M. S. Georgas, A. S. Waterman, J. M. Shainline, R. R. Avizienis, and S. Lin, "Single-chip microprocessor that communicates directly using light," Nature **528**(7583), 534–538 (2015).

2. I. A. Young, E. Mohammed, J. T. Liao, A. M. Kern, S. Palermo, B. A. Block, M. R. Reshotko, and P. L. Chang, "Optical I/O technology for tera-scale computing," IEEE Journal of Solid-State Circuits **45**(1), 235–248 (2009).

3. M. J. Kobrinsky, B. A. Block, J.-F. Zheng, B. C. Barnett, E. Mohammed, M. Reshotko, F. Robertson, S. List, I. Young, and K. Cadien, "On-Chip Optical Interconnects.," Intel Technology Journal **8**(2), 129–141 (2004).

4. J. L. O'brien, A. Furusawa, and J. Vučković, "Photonic quantum technologies," Nature Photonics **3**(12), 687–695 (2009).

5. D. E. Chang, V. Vuletić, and M. D. Lukin, "Quantum nonlinear optics—photon by photon," Nature Photonics **8**(9), 685–694 (2014).

6. T. E. Northup and R. Blatt, "Quantum information transfer using photons," Nature Photonics **8**(5), 356–363 (2014).

7. J. Wang, S. Paesani, Y. Ding, R. Santagati, P. Skrzypczyk, A. Salavrakos, J. Tura, R. Augusiak, L. Mančinska, and D. Bacco, "Multidimensional quantum entanglement with large-scale integrated optics," Science **360**(6386), 285–291 (2018).

8. D. Wang, H. Kelkar, D. Martin-Cano, D. Rattenbacher, A. Shkarin, T. Utikal, S. Götzinger, and V. Sandoghdar, "Turning a molecule into a coherent two-level quantum system," Nature Physics **15**(5), 483–489 (2019).

9. I. Aharonovich, D. Englund, and M. Toth, "Solid-state single-photon emitters," Nature Photonics **10**(10), 631–641 (2016).

10. E. Knill, R. Laflamme, and G. J. Milburn, "A scheme for efficient quantum computation with linear optics," nature **409**(6816), 46–52 (2001).

11. P. Lodahl, "Quantum-dot based photonic quantum networks," Quantum Science and Technology **3**(1), 013001 (2017).

12. L. Vertchenko, N. Akopian, and A. V. Lavrinenko, "Epsilon-Near-Zero Grids for On-chip Quantum Networks," Scientific Reports **9**(1), 1–7 (2019).

13. D. Bouchet, D. Cao, R. Carminati, Y. De Wilde, and V. Krachmalnicoff, "Long-range plasmon-assisted energy transfer between fluorescent emitters," Physical Review Letters **116**(3), 037401 (2016).

14. D. Bouchet, E. Lhuillier, S. Ithurria, A. Gulinatti, I. Rech, R. Carminati, Y. De Wilde, and V. Krachmalnicoff, "Correlated blinking of fluorescent emitters mediated by single plasmons," Physical Review A **95**(3), 033828 (2017).

15. X. He, L. Yang, and T. Yang, "Optical nanofocusing by tapering coupled photonic-plasmonic waveguides," Opt. Express, OE **19**(14), 12865–12872 (2011).

16. Y. Luo, M. Chamanzar, and A. Adibi, "Compact on-chip plasmonic light concentration based on a hybrid photonic-plasmonic structure," Opt. Express, OE **21**(2), 1898–1910 (2013).

17. Y. Luo, M. Chamanzar, A. Apuzzo, R. Salas-Montiel, K. N. Nguyen, S. Blaize, and A. Adibi, "On-chip hybrid photonic–plasmonic light concentrator for nanofocusing in an integrated silicon photonics platform," Nano Letters **15**(2), 849–856 (2015).

18. J. B. Madrigal, R. Tellez-Limon, F. Gardillou, D. Barbier, W. Geng, C. Couteau, R. Salas-Montiel, and S. Blaize, "Hybrid integrated optical waveguides in glass for enhanced visible photoluminescence of nanoemitters," Applied Optics **55**(36), 10263–10268 (2016).

19. D. Vercruysse, P. Neutens, L. Lagae, N. Verellen, and P. Van Dorpe, "Single asymmetric plasmonic antenna as a directional coupler to a dielectric waveguide," ACS Photonics **4**(6), 1398–1402 (2017).

20. D. Vercruysse, Y. Sonnefraud, N. Verellen, F. B. Fuchs, G. Di Martino, L. Lagae, V. V. Moshchalkov, S. A. Maier, and P. Van Dorpe, "Unidirectional Side Scattering of Light by a Single-Element Nanoantenna," Nano Lett. **13**(8), 3843–3849 (2013).

21. J. Li, N. Verellen, D. Vercruysse, T. Bearda, L. Lagae, and P. Van Dorpe, "All-Dielectric Antenna Wavelength Router with Bidirectional Scattering of Visible Light," Nano Lett. **16**(7), 4396–4403 (2016).

22. D. Vercruysse, X. Zheng, Y. Sonnefraud, N. Verellen, G. Di Martino, L. Lagae, G. A. Vandenbosch, V. V. Moshchalkov, S. A. Maier, and P. Van Dorpe, "Directional fluorescence emission by individual V-antennas explained by mode expansion," Acs Nano **8**(8), 8232–8241 (2014).

23. F. Bernal Arango, A. Kwadrin, and A. F. Koenderink, "Plasmonic Antennas Hybridized with Dielectric Waveguides," ACS Nano **6**(11), 10156–10167 (2012).

24. V. Loo, G. Blanquer, M. Joos, Q. Glorieux, Y. De Wilde, and V. Krachmalnicoff, "Imaging light scattered by a subwavelength nanofiber, from near field to far field," Optics Express **27**(2), 350–357 (2019).

25. L. Aigouy, P. Lalanne, J. P. Hugonin, G. Julié, V. Mathet, and M. Mortier, "Near-field analysis of surface waves launched at nanoslit apertures," Physical Review Letters **98**(15), 153902 (2007).

26. X. Xu, A. Broussier, T. Ritacco, M. Nahra, F. Geoffray, A. Issa, S. Jradi, R. Bachelot, C. Couteau, and S. Blaize, "Towards the integration of nanoemitters by direct laser writing on optical glass waveguides," Photonics Research **8**(9), 1541–1550 (2020).

27. C. Deeb, R. Bachelot, J. Plain, A.-L. Baudrion, S. Jradi, A. Bouhelier, O. Soppera, P. K. Jain, L. Huang, and C. Ecoffet, "Quantitative analysis of localized surface plasmons based on molecular probing," ACS Nano **4**(8), 4579–4586 (2010).

28. D. I. Yakubovsky, A. V. Arsenin, Y. V. Stebunov, D. Y. Fedyanin, and V. S. Volkov, "Optical constants and structural properties of thin gold films," Optics Express **25**(21), 25574–25587 (2017).

29. S. Sarkar, V. Gupta, M. Kumar, J. Schubert, P. T. Probst, J. Joseph, and T. A. König, "Hybridized guided-mode resonances via colloidal plasmonic self-assembled grating," ACS Applied Materials & Interfaces **11**(14), 13752–13760 (2019).

30. R. Salas-Montiel, M. Berthel, J. Beltran-Madrigal, S. Huant, A. Drezet, and S. Blaize, "Local density of electromagnetic states in plasmonic nanotapers: spatial resolution limits with nitrogen-vacancy centers in diamond nanospheres," Nanotechnology **28**(20), 205207 (2017).

31. A. B. Vasista and G. P. Kumar, "Quantum emitter coupled to plasmonic nanotriangle: Spatially dependent emission and thermal mapping," Optics Communications **381**, 227–233 (2016).

32. J. Beltran Madrigal, "Integration of a single photon source on a planar dielectric waveguide," Doctoral dissertation, Université de technologie de Troyes (2017).

33. A. Broussier, A. Issa, L. O. Le Cunff, T. H. Nguyen, X. Q. Dinh, S. Blaize, J. Plain, S. Jradi, C. Couteau, and R. Bachelot, "Hybrid plasmonic nanosystem with controlled position of nanoemitters," Applied Physics Letters **114**(16), 163106 (2019).

34. D. Ge, S. Marguet, A. Issa, S. Jradi, T. H. Nguyen, M. Nahra, J. Béal, R. Deturche, H. Chen, and S. Blaize, "Hybrid plasmonic nano-emitters with controlled single quantum emitter positioning on the local excitation field," Nature Communications **11**(1), 1–11 (2020).

SUPPLEMENTAL DOCUMENT

Waveguide efficient directional coupling and decoupling via an integrated plasmonic nanoantenna: supplemental document

S1 – TM MODE DECOUPLING AS A FUNCTION OF LIGHT PROPAGATION DIRECTION IN THE DWG.

Due to the plasmonic nature and the symmetry breaking introduced by the nanotriangle, the intensity of the decoupled light depends on the propagation direction of the guided light in DWG. This is shown by the simulations presented in Figure S1. The simulation frame is sketched in Fig. S1a. The gold nanoantenna is represented in yellow, the TiO_2 DWG in green and the SiO_2 substrate in blue.

As thoroughly shown in [16,17], the nanotriangle decouples mainly the fundamental TM mode that propagates in the DWG. This mode is therefore simulated by Lumerical's source mode in the two possible propagation directions, sketched by the red arrows in Fig. S1a, i.e. either from the base to the apex of the nanotriangle (source I) or vice-versa (source II).
By comparing these two simulations, we can compute the intensity of the radiation decoupled by the structure as a function of the injection direction. Flat monitors M_1 and M_2 are used to record the fraction of the guided light and the box monitor M_R to record the fraction of light decoupled by the nanotriangle and the guided light. These monitors are represented in red on Fig. S2a (drawing not to scale). The intensity of the decoupled light Δ is given by:

$$\Delta = T_R - T_1 - T_2$$

where T_R , T_1 and T_2 are the intensity of the light transmitted throughout M_R, M_1 and M_2 respectively. The intensity of the light decoupled by the plasmonic structure normalized by the injected intensity for both injection direction configurations is shown in Fig. S1b. The dark blue curve is obtained in the "source I" configuration and the light blue curve in the "source II" configuration. As expected, the percentage of light decoupled in the "source I" configuration is larger than the one decoupled in the "source II" configuration in a broad spectral range (from 550 to 660 nm). The agreement with our experimental results obtained 600 nm is good.

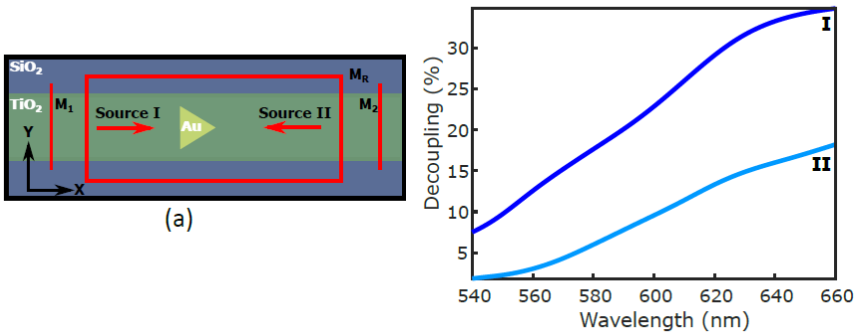

Fig. S1. (a) Sketch of the simulation frame (not to scale). The red lines and the red square represent the monitors $M_{1\,\&\,2}$ and M_R used for simulate the percentage of light decoupled by the gold nanoantenna. The coverslip is represented in blue, the TiO_2 DWG (width = 1 µm, thickness = 150 nm) in green and the gold nanoantenna (base = height= 500 nm) in yellow. Both source mode configurations are represented by the red arrows. (b) Decoupling percentage as a function of the wavelength. The dark blue and light blue curve are calculated in the "source I" and "source II" configurations respectively.

S2 – COUPLING DIPOLE LIGHT MEASUREMENT IN DWG

Flat monitors allow us to measure the optical power of the field which is guided inside the DWG. To this aim, it is crucial to place the flat monitor far enough from the gold nanoantenna. Otherwise, a significant part of the field radiated by the antenna outside the DWG is detected by the flat monitor and artificially increases the measured power. In order to estimate the distance beyond which the uncoupled-field contribution becomes negligible, a simulation, sketched in figure S2a, has been performed. This simulation consists in recording the fraction of coupled light along the DWG thanks to eight flat monitors placed along the DWG, perpendicular to it and regularly spaced by 1µm. The result of this simulation shows that the fraction of coupled light decreases as a function of the distance to the nanoantenna base, until converging at 10µm from the nanoantenna (see figure S2.b). For distances longer than 10µm, the fraction of coupled light in the DWG becomes constant and therefore the power measured by the flat monitors is no longer disturbed by the radiation of the nanoantenna outside the waveguide.

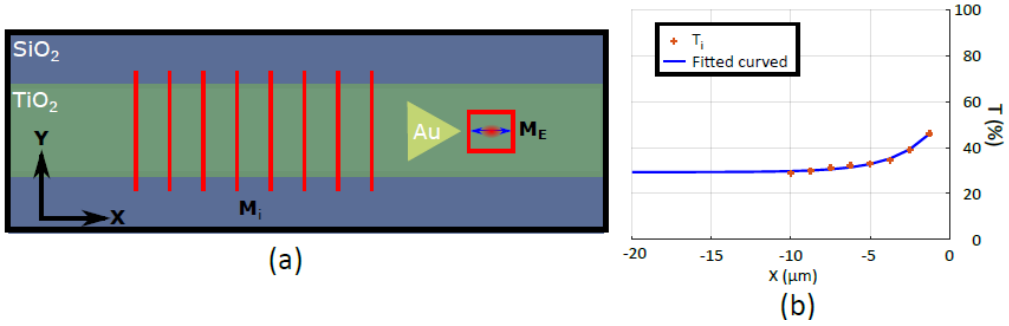

S3 – COUPLING DIPOLE LIGHT BY THE NANOTRIANGLE BASE SIDE

In the main text we report the result of a simulation where a dipole is positioned at the nanotriangle apex. Significant light coupling and directivity is reported under this configuration. To highlight the impact of the dipole position on the light coupling properties of the gold nanotriangle antenna, the same simulation with a dipole located at the nanotriangle base is presented in Figure S3.

The dipole is located 10 nm from the nanotriangle base with an elevation of 55 nm above the DWG surface. Figure S3a shows a preferential light coupling in the DWG towards the apex side of the nanotriangle (red curve) with a transmission close to 7% at 660 nm to be compared to 1% for the other direction (green curve). The situation is reversed with respect to the simulations reported in Fig. 4 a-c of the main manuscript, and the percentage of coupled light is much smaller.

As shown in Figure S3b, the Purcell factor is lower when the dipole is located close to the base of the nanotriangle than when the dipole is located in proximity of the apex. This is the result of a lower dipole coupling efficiency in the first situation with respect to the second one.

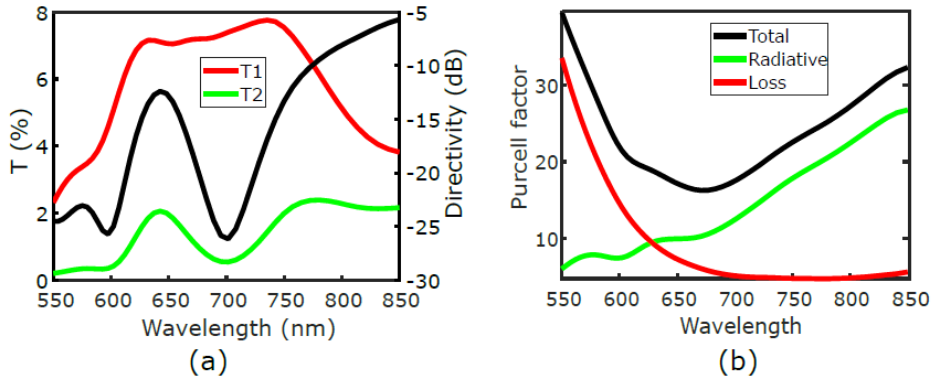

Fig. S3. (a) Simulation results corresponding to the configuration with a dipole located 10 nm from nanotriangle base and $M_{1,2}$ placed 10 μm away from the nanotriangle along the X-axis (see also Fig.4 for the definition of the simulation frame). Green and red plots correspond to the fraction of light coupled in the DWG when the light propagates towards the extremity of the DWG on the base-side and the apex-side of the nanotriangle respectively. Black plot: directivity of the injection in the DWG. (d) Purcell factor (black curve), radiative (green curve) and non-radiative (red curve) components computed for the configuration described in (a).